Published by :
http://www.ijert.org

International Journal of Engineering Research & Technology (IJERT)
ISSN: 2278-0181
Vol. 11 Issue 03, March-2022

Estimation of the Incidence of Liquid Metal Embrittlement Crack in 3rd Generation Advanced High Strength Steel During Resistance Spot Welding using 2D and 3D Weld Lobe Curve

Santhosh Mathi
Institute for Welding and Joining
RWTH Aachen University
Pontstrasse 49, 52062 Aachen, Germany

A. Schiebahn
Institute for Welding and Joining
RWTH Aachen University
Pontstrasse 49, 52062 Aachen, Germany

Pedro Bamberg
Institute for Welding and Joining
RWTH Aachen University
Pontstrasse 49, 52062 Aachen, Germany

U. Reisgen
Institute for Welding and Joining
RWTH Aachen University
Pontstrasse 49, 52062 Aachen, Germany

***Abstract*— Third generation advanced high strength steel (3rd gen AHSS) have been largely used in the automotive industry due to its outstanding mechanical properties. This alloy has the possibility of reducing the vehicle's structural weight by using thinner sheets. Nevertheless, AHSS are more prone to liquid metal embrittlement cracks (LME) due to the zinc (Zn) coating on its surface. Resistance spot welding (RSW) is the most used fabrication process in automotive industry. Avoiding LME cracks during RSW of 3rd gen AHSS is a critical task in the industry which needs to be addressed. Therefore, in this work the critical parameters and its values are estimated for 3rd gen AHSS to produce a defect free weld by generating a weld lobe curve. 3rd generation AHSS type CR850Y1180T was welded with CR4 steel as a counterpart using the RSW process. A list of 202 different process conditions was planned by varying welding current from 4 to 12 kA, welding time from 100 to 1300 ms and electrode force from 2 to 6.5 kN based on a full factorial design of experiment. Quality analyses were made for each welded samples to identify defect and defect free welds (i.e. LME and other defective welds) using stereomicroscope and energy dispersive X-ray spectroscopy (EDS). Scatter plot was generated using MS Excel to plot the output of the welds. As a result, the defect and defect free weld output in the scatter plot are clustered in which weld lobe curve was estimated. Similarly, the 3D plot was made using plotly library in a jupyter notebook which consist of welding current, welding time and electrode force in a three-dimensional space. The resulting 3D plot shows the clear picture of clustering of the defect and defect free weld outputs in a plot. Based on the clustering in the 2D and 3D plot, the weld lobe curve could be prepared, and proper welding parameters were estimated to produce defect free weld in 3rd gen AHSS during RSW process.**

Keywords*— *3rd generation advanced high strength steel, resistance spot welding, design of experiment, weld lobe diagram.

I. INTRODUCTION

Third generation advanced high strength steels (AHSS) have been developed to overcome the drawbacks of the 1st and 2nd generation steels by improving mechanical and metallurgical properties. Third generation AHSS have better formability than 1st generation AHSS of about 60 percent tensile elongation and yield strength above 1200 MPa. Second generation AHSS contains alloying elements that results in 100 percent retained austenite matrix in the material for better strength and formability. Nevertheless, it has a problem of delayed cracking during service condition. Moreover, increase in alloying contents will increase the cost of the steel product. Therefore, the 3rd generation AHSS have been developed with reduced alloying elements. It contains above 20 percent of retained austenite in the ferrite/martensite matrix. This matrix is attained by the novel heat treatment process route of carbon partitioning to achieve less retained austenite in the matrix unlike 2nd generation AHSS. [1]

Resistance spot welding is a process of joining two overlapped metal sheets by passing electric current through the contacting welding electrodes, applying pressure to the sheets. The electric current converted into heat energy along with compressive force on both sides of the metal sheets overlapped lead to the formation of a weld spot (nugget) between them. The process works based on the principle of Joule's law of heating (Q), shown by the Equation 1.

$$Q = I^2 . R . t \quad (1)$$

Where, 'I' is the electric current passed through the weld spot, in Amperes, 'R' is the contact resistance, in Ohm, and 't' is the welding time, in milliseconds. [2, 3]

RSW is an important manufacturing process used in the automotive industries to fabricate a vehicle. Around 3000 to 6000 weld spots are made on automotive structure, parts and components. Implementing 3rd generation AHSS in RSW

International Journal of Engineering Research & Technology (IJERT)
ISSN: 2278-0181
Vol. 11 Issue 03, March-2022

process plays a major role in weight reduction and fuel consumption in automotive. [4, 5] Nevertheless, the liquid metal embrittlement crack is the phenomenon of crack formation in a solid metal when a liquid metal encounter solid metal at a critical temperature and pressure. AHSS are coated with zinc on the surface for corrosion resistance purposes, which melts during RSW process at a critical temperature (i.e., above melting point of zinc) and critical pressure (i.e., above yield point of the material). [6] The molten zinc on the surface infiltrates into the grain boundaries of welding sheet, what decreases the ductility of the material and leads to liquid metal embrittlement cracks. [7] This is a major problem which limits the application of 3rd generation AHSS in RSW process that needs to be addressed. The formation of LME crack is influenced by various factors such as material related parameters, process parameters and type of zinc coating. Therefore, understanding the LME crack formation and preventing the crack is still a challenging task to the researchers and industrial experts. [8]

Several works from literature based on the different parameters that influence the formation of LME crack in AHSS during the RSW process were published in recent years. For instance, the strength of the TRIP1100 steel has decreased in a tested sample on average of 25% due to the location of the crack between coated and uncoated steel [9]. Literature [10] monitored the fracture path of inner crack in the welded 3rd gen AHSS by conducting interrupted cross tension and tensile shear test. The LME sensitivity for galvanized Q&P 980 steel (one of the types of 3rd gen AHSS) had been investigated and it was found that the LME susceptibility increased with higher welding current and prolonged welding time. [11] The influence of electrode geometry for galvannealed TRIP steel was studied and concluded that the LME cracks are more likely to form in dome-type electrodes than flat electrodes. [12] The influence of different types of zinc coating in the formation of LME in TWIP steels was investigated. Hot-dip galvanized zinc coating has the least susceptibility to LME formation than electro-galvanized and hot-dip galvannealed zinc coating. [8, 13] The operating range of welding parameters for TRIP800 steel was developed by varying welding time and welding current to produce spot weld without LME crack. [14]

This project aims to identify a process window to distinguish allowable and LME crack zone for the resistance spot welded 3rd generation AHSS sheet with 1.2 mm thickness. Welded samples are analyzed with stereo microscope and categorized the defective welds such as LME, insufficient nugget diameter and splash. A 2D weld lobe is drawn from the scatter plot based on the most influencing process parameters such as welding current, welding time and electrode force to identify the LME crack zone in the weld lobe. Using python library, a 3D plot is made with welding current, welding time and electrode force in x, y and z axis respectively. By using the graph, the LME predominant zone could be identified in the 2D and 3D weld lobe for RSW process. This work can serve as a reference for future industrial use related to the join of 3rd generation AHSS using RSW processes. Moreover, it could be a supporting material for researchers to understand theoretically the relationship between the most influencing parameters and the formation of LME crack.

II. EXPERIMENTAL DETAILS

A. Material

The third-generation advanced high strength steel grade CR850Y1180T, or DP1200, with a sheet thickness of approximately 1.20 mm, was used in the experiment. The CR850Y1180T alloy denotes a cold rolled steel with 850 Mpa yield strength and 1180 Mpa ultimate tensile strength. Along with the AHSS, CR4 grade steel with a thickness of approximately 0.8 mm is used as a counterpart. Both steel sheets are Zn-coated with a layer thickness of approximately 5 µm. The composition of the CR850Y1180T and CR4 material is shown in the Table I.

Table I: Chemical composition of CR850Y1180 and CR4 steel

	C	Si	Mn	P	S	Cr
CR850Y 1180T	0.219	1.49	2.43	0.0075	0.0028	0.0723
CR4	0.0103	0.0173	0.0956	0.0088	0.0087	0.0275

	Mo	Ni	Al	Co	Cu	Fe
CR850Y 1180T	0.0750	0.0195	0.0524	0.0247	0.0145	95.6
CR4	0.0071	0.0257	0.0428	0.0100	0.0143	99.5

B. Equipment and Parameters

The RSW process is performed using a C-type welding gun from Fronius International with a 1000 Hz medium frequency direct current (MFDC) transformer, shown in Fig 1. Dissimilar metals such as CR850Y1180T (3rd gen AHSS type steel) and CR4 (Mild steel) sheets were prepared with dimensions of 45 × 45 mm and resistance spot welded. The electrodes were cooled using water with a flow rate of 4 litres/minute.

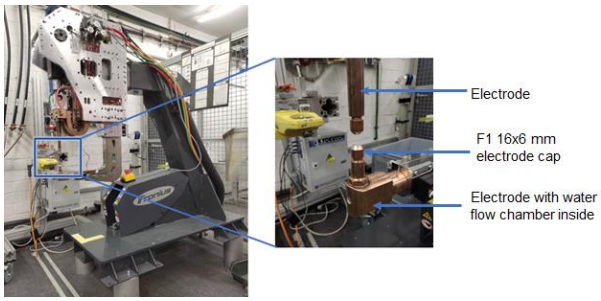

Figure 1: Fronius 'C-type' resistance spot welding machine along with F1 16*6 mm electrode caps

After preparing 50 welds, the electrode caps were milled to avoid the influence of the oxide layer in the LME formation. A dome type F1 16x6 mm electrode cap was used in the complete experimental work, as per the reference from ISO5821:2009, based on the sheet thickness.

International Journal of Engineering Research & Technology (IJERT)
ISSN: 2278-0181
Vol. 11 Issue 03, March-2022

C. RSW Process Setup

CR850Y1180T sheet with 1.2 mm thickness was positioned at the top and the CR4 sheet with 0.8 mm thickness was placed at the bottom during spot welding. The sheets were overlapped with 40 x 40 mm and welded with one single central spot weld without a shunt, shown in Fig 2.

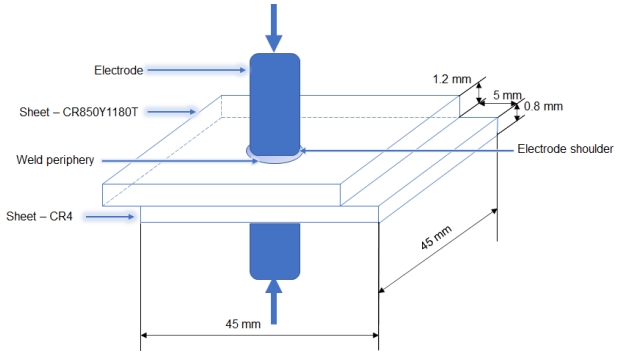

Figure 2: Spot welding sheet setup

D. Design of Experiment

Based on the literature study [2, 4, 8] the most influencing process-related parameters like welding current, welding time and electrode force are varied for investigation. On the other hand, material-related parameters like material type, coating type, material thickness were fixed. Similarly, the electrode cap (F1 16x6 mm) and the other process parameters like hold time as 120 milliseconds and squeeze time as 150 milliseconds were also fixed. The ranges of values of the chosen parameters used in each phase of the experimental work are shown in Table II. The experimental work was conducted in four phases for easy characterization and analysis.

Table II: Magnitude of parameters used in the experiment

Work phase	Parameters	Range of Values
Phase 1 (25 x 3 = 75) welds	Welding current [kA]	7.8
	Welding time [ms]	100, 200, 300, 400, 500
	Electrode force	2, 3, 4, 5, 6
Phase 2 (24 x 3 = 72) welds	Welding current [kA]	4, 6, 8, 10, 12
	Welding time [ms]	100, 300, 600, 900, 1200
	Electrode force	1, 3, 5, 7
Phase 3 (63 x 3 = 189) welds	Welding current [kA]	5.6, 7.2, 8.8, 10.4, 12
	Welding time [ms]	100, 400, 700, 1000, 1300
	Electrode force	2, 3.5, 5, 6.5
Phase 4 (90 x 3 = 270) welds	Welding current [kA]	5, 6, 7, 8, 9 kA
	Welding time [ms]	200, 300, 400, 500, 600, 700 ms
	Electrode force	3, 4, 5 kN

Note: In phases 2 and 3, some parameter combinations (i.e., high current with high weld time) with an apparent splash incidence are omitted. Thus, 202 data points were planned, and 606 weld spots weld samples were made for measurement and analysis considering three repetitions to avoid misinterpretation.

Full Factorial Design of Experiment

Fig 3 shows a three-dimensional cube with the range of chosen process parameters used in the work phase 4. The welding current ranges from 5 to 9 kA with 1 kA steps was kept x-axis. A welding time from 200 to 700 ms was increased in steps of 100 ms was in the y-axis, and electrode force from 3 to 5 kN with 1 kN steps was in the z-axis. Samples are welded by varying the current, time and force within this range of all possible combinations as per the full factorial design of the experiment, shown in Fig 4. The idea is to determine the output category of sample for a wide range of chosen process parameters space inside the 3D box. If the data points with the same output category are clustered at a particular region, a weld lode curve could be drawn to distinguish the acceptable and defective welds.

For instance, the first circle on the left in Fig 4 represents electrode forces 3, 4 and 5 kN. The second circle represents weld current with five steps and the third circle as weld time with six steps. The experiments proceed with a combination of values like (3, 5, 200), (3, 5, 300) and then (3,6,200), (3,6,300) and it goes similarly for the possible combination of all values in these three circles. Thus, the first value represents electrode force, the second value is weld current and the third value is weld time.

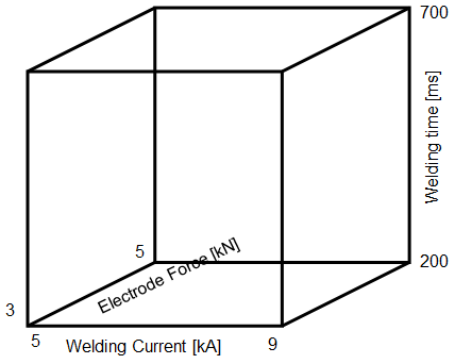

Figure 3: Three-dimensional parameter range for the full factorial design of the experiment

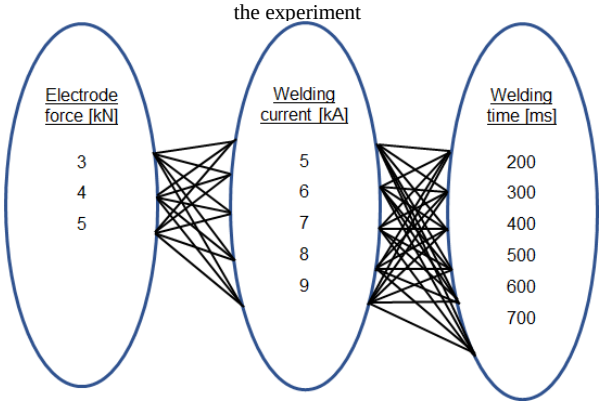

Figure 4: All possible combinations of values from the chosen process parameters

International Journal of Engineering Research & Technology (IJERT)
ISSN: 2278-0181
Vol. 11 Issue 03, March-2022

A 3x5x6 = 90 parameters combination was implemented in phase 4 to observe the incidence of splash and LME. Including all the four phases, 202 parameter combinations (i.e. Data points) were planned. Three repetitions were made for each weld parameter combination to avoid the experimental error. Therefore, a total of 606 spot weld samples were produced for the study in the project work. A wide range of parameter values was chosen, not to omit any space (i.e. input parameters and corresponding output) inside the 3D box that could cause LME crack formation. The idea helps understand the relationship between the parameters extensively.

E. Measurement and Analysis

LME Incidence Analysis

Welded samples are analyzed on both (CR850Y1180T and CR4) sides of sheet surface using a stereomicroscope to identify the incidence of LME crack, shown in Fig 5. First, the samples are cross sectioned at the center of the nugget to confirm the presence of zinc inside the grain boundary using EDS analysis. The position of the plane for the sample cross-section is shown in Fig 6. Before taking to the stereomicroscope, the welded samples are etched using an etchant to remove the zinc coating on the surface. It helps to reveal the crack more visibly and avoid misunderstanding the zinc oxide as a crack. The etchant was made of 500 ml (hydrochloric acid), 500 ml (distilled water) and 3.5 g (Hexamethylenetetramine). The samples are dipped into the etchant for few minutes until the bubbling stopped. Then, it is washed by dipping into the water in another beaker and then dried properly. The sample identified with the crack line similarly like in Fig 7 and the presence of zinc in the crack line was confirmed using EDS analysis which is considered as an 'LME' category sample.

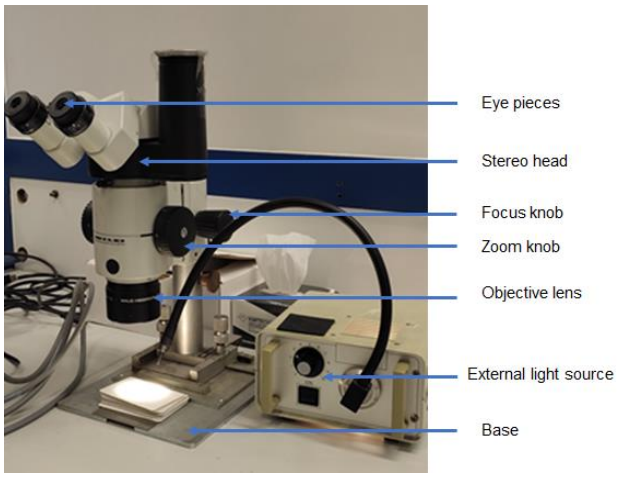

Figure 5: Stereo Microscope with an external light source

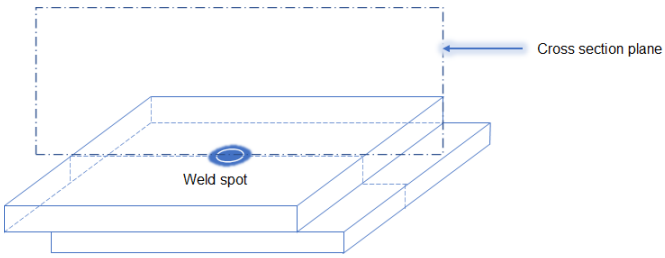

Figure 6: Cross-section position of welded sample for EDS analysis

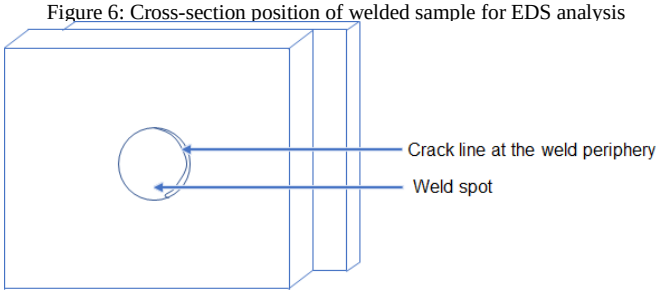

Figure 7: Front view of the welded sample with a crack line at the periphery of the weld spot

Nugget Size Measurement

One sample from each parameter combination (i.e., 202 samples) was opened using a chisel to measure the nugget diameter. The nugget diameter in a sample was measured in two positions by turning the vernier calipers into 90° and the average diameter was taken. The minimum size of the nugget should be $d_{min}>4\sqrt{T}$, as per 'American National Standard' ANSI/AWS/SAE/D8.9-97, Section 5.7:1997 to produce strong and acceptable welds. The thickness of the CR4 sheet was considered and the minimum allowable nugget diameter was calculated as $4\sqrt{(0.8)}$, which is equal to 3.577 mm. Therefore, the nugget diameter less than 3.577 mm, was considered the 'Insufficient nugget size' category.

Splash Incidence analysis

Splashes in each sample were observed at the time of welding. Splash could be easily identified by observing the spark due to the ejection/expulsion of metals during the welding. Therefore, the sample with an incidence of expulsion during welding was noted as the 'splash/spatter' category. Once two sheets are opened using a chisel, splash could be more easily identified. The traces of ejection of liquid metal from the nugget or broken nugget confirms the incidence of spatter in the sample.

Electric Resistance Measurement

The theoretical relationship between welding current, welding time and electrode force in the formation of LME was investigated based on Joule's law of heating. The idea is to relate Joule's law of heating with electrode force. Therefore, the theoretical relationship between welding current, welding time and electrode force are quantified. Here, the welding current and welding time was already a known input parameter from the experiment. Therefore, resistance is the only parameter that needs to be measured to interpret Joule's law. As per the guidance of 'ISO 18594 – Resistance spot-,

International Journal of Engineering Research & Technology (IJERT)
ISSN: 2278-0181
Vol. 11 Issue 03, March-2022

projection- and seam welding – Method for determining the transition resistance on aluminium and steel material,' the current and voltage was measured at two different spots directly on the welding sheets and then the resistance was calculated using the measured voltage and current values.

A compact welding monitor was used to measure the voltage at the two different points before and after the welding. Subsequently, a voltage drops or the difference between the voltage at two spots along with the current measurement gave resistance values between two points of connected cables. Likewise, the resistance was observed for each weld and the data was exported in excel format. The measured resistance includes contacting resistance between two sheets, bulk resistance of each sheet and the contact resistance between sheet and electrode. The electric resistance measurement setup overview is shown in Fig 8.

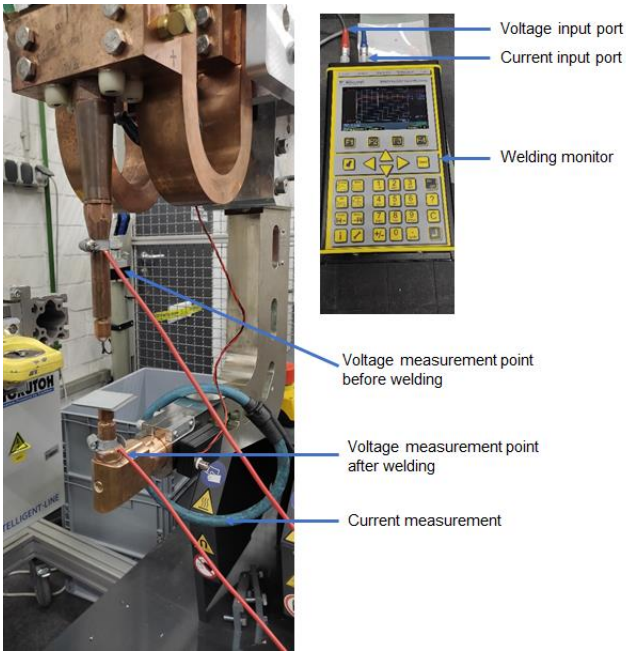

Figure 8: Resistance measurement setup

III. Results and Discussion

The experimental data were interpreted and investigated regarding LME formation by generating the weld lobe. The generated results show the operating range of welding parameters for the selected process condition in this work. Furthermore, it establishes the correlations between the desired goal to estimate the proneness of LME cracking in 3rd generation AHSS and to produce LME crack free spot welds.

A. Confirmation of LME Crack incidence

The samples without LME crack and with LME crack are shown in Fig 9 and Fig 10 respectively. In Fig 10, the red mark shows a crack line in the CR850Y1180T steel surface at the weld spot. It was observed that the LME crack was only formed in CR850Y1180 steel. There was no incidence of LME in the counterpart, the CR4 steel.

Figure 9: Welded sample without crack

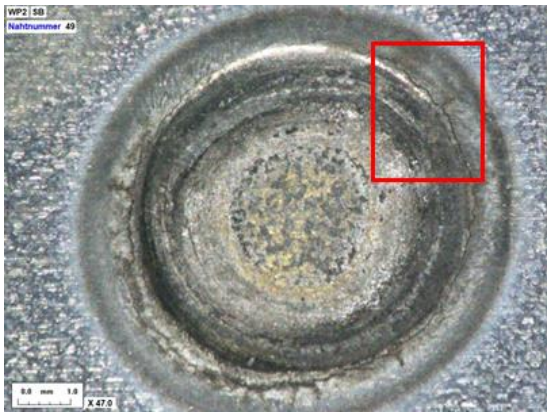

Figure 10: Incidence of crack at the periphery of the weld spot marked in a red box

Then, the samples identified with cracks are taken to EDS analysis to check the presence of zinc in the grain boundaries. A sample cross-section with an LME-crack is highlighted by the red mark shown in Fig 11. EDS analysis shows the presence of zinc (Zn marked in light blue color) in the crack wall shown in Fig 12.

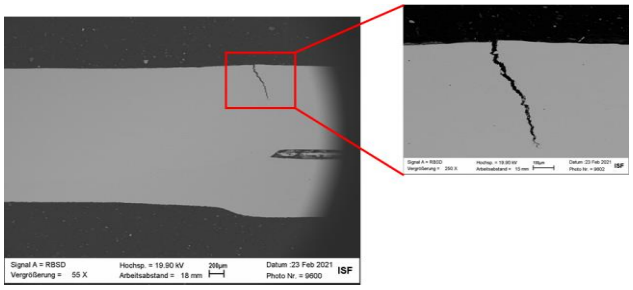

Figure 11: Cross-section of weld sample along with the incidence of crack

International Journal of Engineering Research & Technology (IJERT)
ISSN: 2278-0181
Vol. 11 Issue 03, March-2022

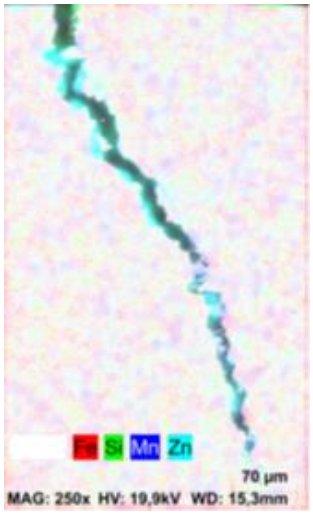

Figure 12: Zinc filled inside the crack from EDS analysis

It was observed that the AHSS steel that has a strength of 1180 Mpa (i.e., >1000 Mpa) is more prone to LME crack than the mild steel that has strength less than 1000 Mpa, which correlates with the study of reference [15]. Furthermore, the presence of a higher amount of Si and Al in CR850Y1180T steel may increases its bulk resistance. As a result, heat generation due to resistance could be higher in CR850Y1180T steel than the CR4 steel, which could cause LME formation more predominant, as mentioned correlates with reference [8].

B. Effects of Parameters in LME formation

Fig 13 shows the cross-section of welded samples and the incidence of the crack in CR850Y1180T steel at the magnification of 2.5x. The welding parameters are informed in each image. LME cracks are more predominant in the samples with electrode force less than 3 kN and weld current above 8 kA. All the cracks are located at the electrode cap shoulders (i.e., the periphery of the weld spot).

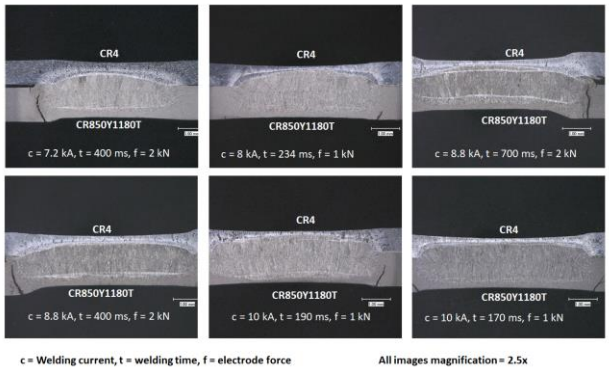

Figure 13: Cross-section of welded samples with LME crack incidence only in CR850Y1180T steel

LME cracks are predominant in the sample, with a significant portion of nugget height contains CR850Y1180T steel. Fig 14b and Fig 14d shows that the sample with the incidence of LME crack has less height of CR4 steel than the CR850Y1180T steel. The height ratio of CR850Y1180T was calculated by measuring the individual height of contributing metals at the weld spot using the Equation 2.

$$\text{Hratio (b)} = \frac{\text{hb}}{(\text{ha} + \text{hb})} \tag{2}$$

Where 'h_a' represents the height of the CR4 steel sheet, 'h_b' denotes the height of the CR850Y1180T steel sheet and 'H_{ratio} (b)' is the ratio of the height of CR850Y1180 steel sheet at weld spot.

The LME crack samples have the ratio of CR850Y1180T steel between 0.89 and 0.91, shown in Fig 14b and Fig 14d, respectively. Similarly, the sample without LME crack has a ratio between 0.58 and 0.68, shown in Fig14a and Fig 14c, respectively. Therefore, the ratio of nugget height of high strength steel above 0.80 in the welded sample clearly shows the incidence of LME.

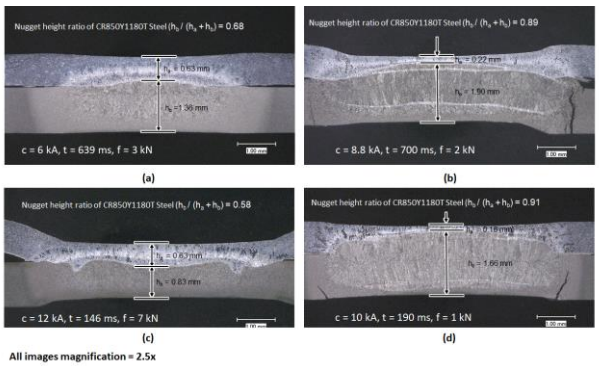

Figure 14: Comparison of nugget height ratio between steels contains LME and Non-LME cracks

Fig 15 shows the welded samples with LME crack at the periphery of the weld spot marked with a red line for reference. The welding parameters that primarily influences the incidence of LME in this study shows the combination of lower electrode force from 1 to 3.5 kN along with welding current higher than 5.8 kA. Fig 16 shows the sample without LME cracks which has higher electrode force between 4-7 kN and welding current 6-8 kA combination that produces good weld samples. Electrode force (4-7 kN) with current (9-12 kN) predominantly produces samples with a splash. But, the welding current between 8 and 9 kN for the same electrode force was not so stable. For instance, out of three samples, there was an incidence of a crack in one sample but not in the others. Similarly, welding currents lower than 5.8 kA produce weld nuggets smaller than the minimum allowable diameter. The samples with LME or splash are evident for the influence of electrode force (below 4kN) to produce defective welds in this work.

International Journal of Engineering Research & Technology (IJERT)
ISSN: 2278-0181
Vol. 11 Issue 03, March-2022

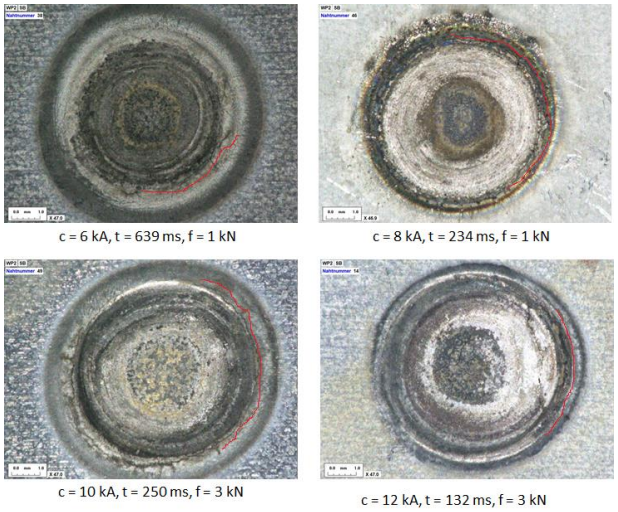

Figure 15: LME crack at the periphery of the weld spot along with its parameters

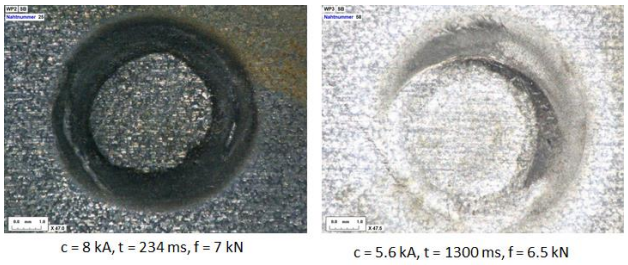

Figure 16: Samples without LME crack

It was found that every sample with the incidence of LME cracks has a larger nugget size ratio, while the sample without crack has a smaller nugget size ratio. Whereas nugget size ratio (h_n/d_n) is the ratio of nugget height (h_n) and nugget diameter (d_n). Fig 17 shows the dimensions of the nugget in a sample with LME crack and its nugget size ratio was estimated as 0.125 mm. However, the nugget size ratio of the sample without crack was estimated as 0.0435 mm, which is almost three times smaller than the previous one, shown in Fig 18.

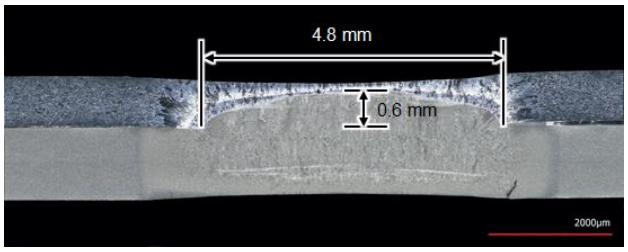

Figure 17: Nugget size of the sample with LME crack with (h_n/d_n) = 0.125 mm

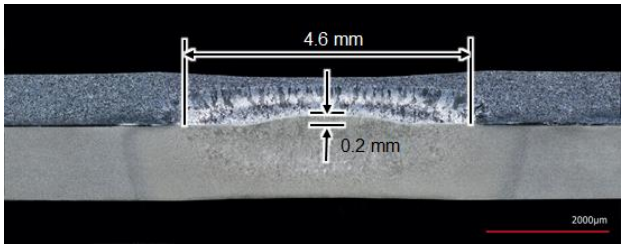

Figure 18: Nugget size of the sample without LME crack with (h_n/d_n) = 0.0435 mm

C. Theoretical Interpretation of LME crack formation

Resistance induced in each sample (i.e. 270 samples) during work phase 4 was measured using a welding monitor and the values are plotted and shown in Fig 19. The curve shows the resistance values measured during welding for all the 270 samples. The standard deviation of all the samples was calculated as 31.6363 µm. Furthermore, it shows that the chosen three different electrode forces 3, 4, 5 kN do not show considerable deviations on the electric resistance generated on the sample. Nevertheless, the relationship between the three electrode forces and the resistance had found in the scatter plot, shown in Fig 20.

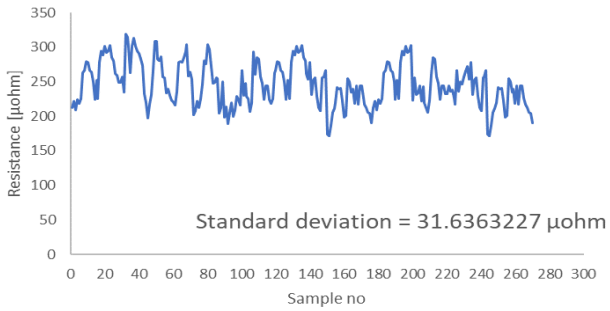

Figure 19: Resistance induced during RSW for each sample in work phase 4

The minimum resistance is attained during 3 kN electrode force was around 200µohm and for 5 kN electrode force, the resistance starts from 170 µohm. Similarly, the maximum value of resistance for 3 kN and 5 kN was around 300 µohm and 270 µohm, respectively. Therefore, the increased electrode force had decreased contact resistance and heat input between the sheets welded and it correlates with [16, 17]. It is inferred that, using a lower electrode force (i.e., 3 kN), the compressive force applied to the weld spot should be comparatively less. The reason could be the presence of small air gaps, due to the irregular surfaces contact between electrode and sheet and between both sheets as well, shown in Fig 21, generating higher electric resistance. Similarly, under higher electrode force, due to increased compressive force, the air gaps between electrode and sheets are likely to close and thus lower contact resistance and heat input is identified, what can be also found in the literature [8, 18]

International Journal of Engineering Research & Technology (IJERT)
ISSN: 2278-0181
Vol. 11 Issue 03, March-2022

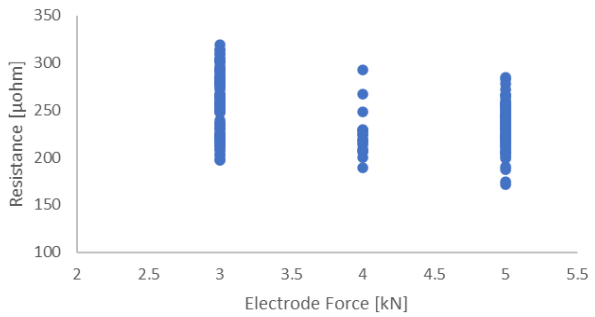

Figure 20: Relation between electrode and resistance induced in each sample in work phase 4

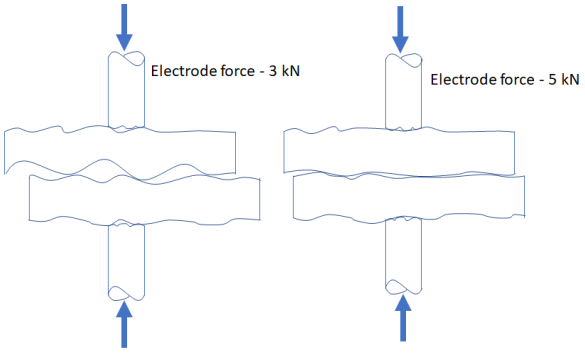

Figure 21: Influence of electrode force in surface clearance

The Joule's heat input (Q) was calculated based on the resistance measured. Temperature (T2) induced in the weld sample was calculated using the specific heat capacity formula shown in Equation 3. The specific heat capacity of the material was considered as 486 J/Kg.K [19].

$$Q = m \times Cp \times (T2-T1) \quad (3)$$

Where 'm' represents the mass of the sample, C_p the specific heat capacity of the weld material in [J/Kg.K] and T1 and T2 represent the initial and final temperature in Kelvin [K], respectively.

The induced heat in the weld sample was converted into a temperature that occurred during welding for better quantification. Therefore, the relation between the temperature and the electrode force was plotted using a scatter plot based on the welded sample's output category and shown in Fig 22. It shows that higher electrode force like 4 to 5 kN can produce good welds even at a higher temperature range 850 to 900 °C, unlike lower electrode force. On the other hand, lower electrode force (i.e., 3 kN) with high temperature produced more LME crack samples.

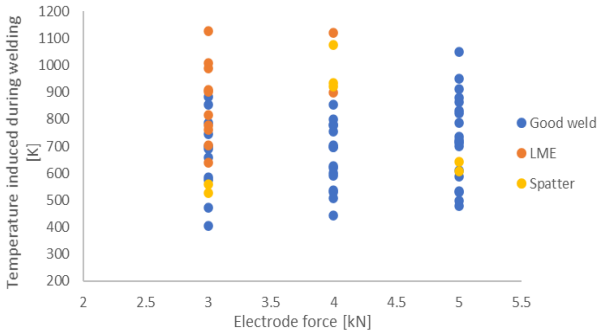

Figure 22: Relation between temperature-induced in the weld sample and the electrode force used for each sample

D. Generation of 2D Weld Lobe

Weld lobe curve was drawn in the scatter plot from the experimental data obtained from work phase 4. Each data point from experimental data contains a combination of process parameter values (weld current, weld time and electrode force) and corresponding output category. The scatter plot was made by indicating different colors for each category. Weld lobe curve was estimated by varying welding current (in X-axis) and welding time (Y-axis) with fixed electrode force. Similarly, scatter plots were made for three different fixed electrode forces (3 kN, 4 kN and 5 kN) along with varied welding current and welding time shown in the Fig 23, Fig 24 and Fig 25. Based on the observation, the left boundary of the weld lobe diagram was determined by minimum allowable nugget diameter as per 'American National Standard' ANSI/AWS/SAE/D8.9-97, Section 5.7:1997. The incidence of splash and LME limits the right boundary of the weld lobe diagram. The top of the right-handed side boundary was identified as the LME region where many LME samples were identified which is shown in orange color. The bottom right-hand side boundary was identified as a splash region with more samples found with expulsion in the weld nugget. There is no obvious/stable boundary between LME and splash region in the weld lobe graph because few samples with the splash category lie in the LME dominant region. Similarly, some samples with the LME category lie in the splash dominant region.

Fig 23 shows the weld lobe for electrode force of 3 kN in which the good weld was possibly made at welding current between 6 and 7 kA. Similarly, the good welds are reliably produced at a weld time starting from 400 ms until 700 ms. The LME dominant samples are predominant at the region where welding current was above 8 kA and welding time above 300 ms.

International Journal of Engineering Research & Technology (IJERT)
ISSN: 2278-0181
Vol. 11 Issue 03, March-2022

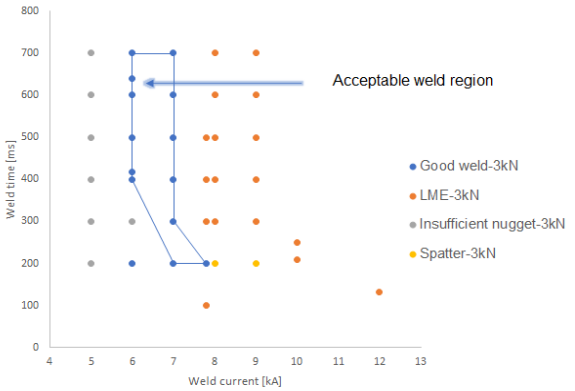

Figure 23: Weld lobe for electrode for 3kN

Fig 24 shows the weld lobe curve for fixed electrode force of 4 kN with varied welding current and welding time. Compared to Fig 23, the welding current range has moved to right-hand side between 7 and 8 kN. It is inferred that the welding current range to produce good welds had increased due to increased electrode force. The defect free welds could be produced with a welding time starting from 200 ms to 700 ms. Therefore, the electrode force of 4 kN has the larger range of welding time compared to 3 kN electrode force. The spatter samples represented by the yellow color dots are also identified in the region of welding current above 8 kN and welding time from 200 to 600 ms. Unlike Fig 23 shows, LME samples are more predominant than spatter samples. Therefore, electrode force of 4 kN produced welds with lesser LME and more spatter samples than 3 kN electrode force at same range of welding current and welding time.

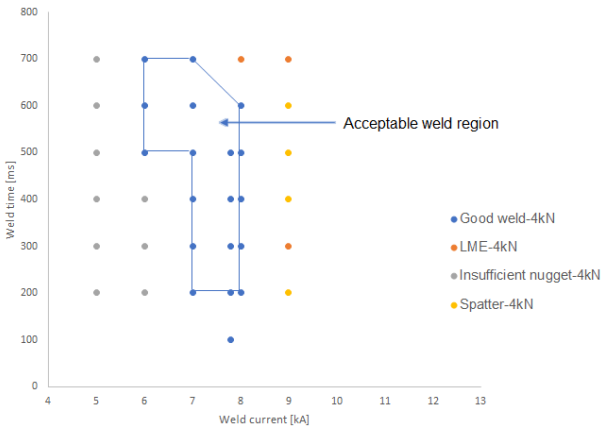

Figure 24: Weld lobe for electrode for 4kN

Fig 25 shows the weld lobe curve for electrode force 5 kN. Here the weld lobe curve is almost like previous figure. The welding current range to produce defect free welds lies in the range of 7 to 8 kA and welding time between 300 to 700 ms. In this figure, there are more spatter samples are found at welding current of 8 kA compared to previous weld lobe curves.

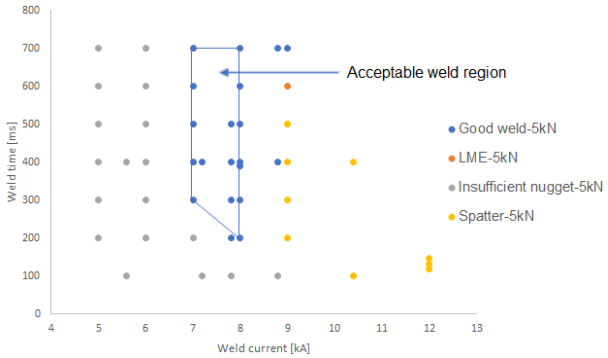

Figure 25: Weld lobe for electrode for 5kN

Fig 26 shows the comparison of the weld lobe for electrode force 3, 4, 5 kN. The threshold value of welding current under the selected process conditions for electrode force of 3, 4 and 5 kN settings is 7.8 kA without a splash. Therefore, the welding current required to produce a 'Good weld' is between 6 and 7 kA with electrode force 3 and 4 kN. But, for electrode force 5 kN, the allowable welding current is between 7 and 8 kA, in which the border moved to the right. This phenomenon is due to the decrease in contact resistance while the RSW process with higher electrode force correlates with Ref. [16]. A high welding current with lower electrode force tends to generate more heat, which causes the incidence of severe splashes. Therefore, increasing electrode force will help avoid splash, which complies with reference [20]. Higher electrode force like 4 and 5 kN shows larger range of welding current and welding to produce defect free welds compared to 3 kN electrode force.

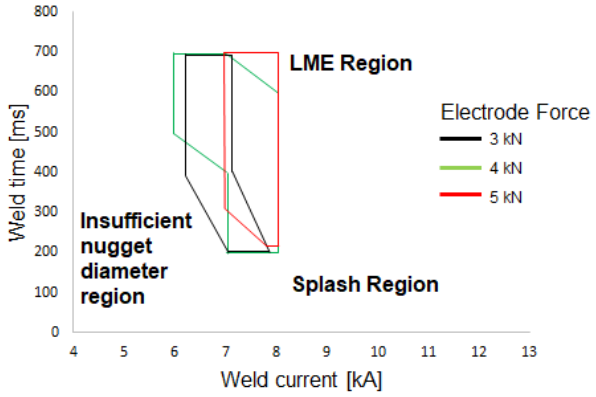

Figure 26: Weld lobe comparison between electrode force 3, 4 and 5 kN

E. Generation of 3D Weld Lobe

Three-dimensional scatter plot was made using a graphing library called 'Plotly' in a jupyter notebook. The experimental data points and its output category are plotted and shown in the Fig 27. The plotted result shows the three-dimensional view consists of three process parameters of welding current, welding time and electrode force in x, y and z axis respectively. Two different angles are show in the figure to visualize the clustering of LME sample data points and 'Good weld' sample data points. LME category samples shown in red color dots are clustered in the graph which indicates LME

International Journal of Engineering Research & Technology (IJERT)
ISSN: 2278-0181
Vol. 11 Issue 03, March-2022

dominant zone. In the diagram, the LME is dominant in at lower electrode force below 3 kN, welding current between 8 to 10 kN. Higher electrode force and higher welding current had larger number of splash/spatter samples. Lower electrode force and higher welding current had many LME samples. Insufficient nugget diameter was predominant in the region at higher electrode force and lower welding current which correlates with the 2D weld lobe. Based on the generated 3D weld lobe, the region for producing defect free welds and LME welds were clustered and the operating parameters were identified.

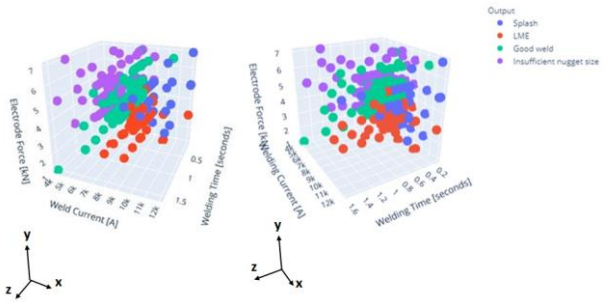

Figure 27: 3D plot showing datapoints with output categories in a different color

IV. CONCLUSION

The estimation of LME incidence from the weld lobe needs a sensitive data collected from the experimental work. The sensitive data contains list of data points with relationship between input and output. Based on the clustering of output categories, weld lobe could be drawn and the zone of particular category (i.e., LME and LME free zones) were estimated. According to the results of the present work, an alternative way to demonstrate weld lobes was drawn and several conclusions have been made:

- LME crack is more predominant in CR850Y1180T (> 1000 MPa) than in CR4 (< 1000 MPa).
- A larger height ratio Hratio of CR850Y1180T steel of above 0.8 in weld nugget has LME incidence.
- LME is more prone when there is a higher current (>7.8 kA) and lower electrode force (<3 kN) combination. As mentioned in section C, lower electrode force generates higher contact resistance in the weld sample. Additionally, at a higher current with lower electrode force, the temperature in the weld zone increases above a critical temperature, leading to the formation of LME crack.
- Higher electrode force (4-7 kN) inhibits LME crack at higher current till 7.8 kA of weld current.
- The safe range of working parameters for the chosen materials and process conditions are said to be welding current as 7 to 7.8 kA and welding time is 250 to 300 ms with electrode force of 3 to 5 kN.

REFERENCES

[1] W. Bleck, F. Brühl, Y. Ma, and C. Sasse, “Materials and Processes for the Third-generation Advanced High-strength Steels,” Berg Huettenmaenn Monatsh, vol. 164, no. 11, pp. 466–474, 2019.

[2] M. Biegler, C. Böhne, J. Frei, G. Meschut, and M. Rethmeier, “Prevention of liquid metal embrittlement cracks in resistance spot welds by adaption of electrode geometry,” Science and Technology of Welding and Joining, vol. 25, no. 4, pp. 303–310, 2020.

[3] J. H. Schmitt and T. Iung, “New developments of advanced high-strength steels for automotive applications,” Comptes Rendus Physique, 2018.

[4] P. Arjun Dhawale and Kulkarni M L, “Electric Resistance Spot Welding: A State of Art,” International Journal of Engineering Research & Technology (IJERT), vol. 5, no. 1, 2017.

[5] X. Zhang, G. Chen, Y. Zhang, and X. Lai, “Improvement of resistance spot weldability for dual-phase (DP600) steels using servo gun,” Journal of Materials Processing Technology, vol. 209, no. 5, pp. 2671–2675, 2009, doi: 10.1016/j.jmatprotec.2008.06.008.

[6] Z. Ling, T. Chen, L. Kong, M. Wang, H. Pan, and M. Lei, “Liquid Metal Embrittlement Cracking During Resistance Spot Welding of Galvanized Q&P980 Steel,” Metall Mater Trans A, vol. 50, no. 11, 2019, doi: 10.1007/s11661-019-05388-6.

[7] M. Nicholas and C. F. Old, “Review Liquid metal embrittlement,” 1979.

[8] D. Bhattacharya, “Liquid metal embrittlement during resistance spot welding of Zn-coated high-strength steels,” Materials Science and Technology, vol. 34, no. 15, pp. 1809–1829, 2018, doi: 10.1080/02670836.2018.1461595.

[9] C. DiGiovanni, X. Han, A. Powell, E. Biro, and NY. Zhou, “Experimental and numerical analysis of liquid metal embrittlement crack location,” Journal of Materials Engineering and Performance, 28(4):2045–2052, 2019.

[10] O. Siar, S. Dancette, T. Dupuy, and D. Fabrègue, “Impact of liquid metal embrittlement inner cracks on the mechanical behavior of 3rd generation advanced high strength steel spot welds,” Journal of Materials Research and Technology, 15:6678–6689, 2021.

[11] Z. Ling, M. Wang, L. Kong, and K. Chen, “Towards an explanation of liquid metal embrittlement cracking in resistance spot welding of dissimilar steels,” Materials & Design, 195:109055, 2020.

[12] S. P. Murugan, K. Mahmud, C. Ji, I. Jo, and Y.-D. Park, “Critical design parameters of the electrode for liquid metal embrittlement cracking in resistance spot welding,” Weld World, vol. 63, no. 6, pp. 1613–1632, 2019, doi: 10.1007/s40194-019-00797-y.

[13] R. Ashiri, M. Haque, C. Ji, H. R. Salimijazi, Y. Park, et al. Supercritical area and critical nugget diameter for liquid metal embrittlement of zn-coated twining induced plasticity steels. Scripta Materialia, 109: 6–10, 2015.

[14] H. Emre and R. Kaçar. Development of weld lobe for resistance spot-welded trip800 steel and evaluation of fracture mode of its weldment. The International Journal of Advanced Manufacturing Technology, 83(9-12):1737–1747, 2016.

[15] Z. Ling, M. Wang, L. Kong, and Ke. Chen, “Towards an explanation of liquid metal embrittlement cracking in resistance spot welding of dissimilar steels,” Materials & Design, 195:109055, 2020.

[16] E. Wintjes et al., “Effect of Multiple Pulse Resistance Spot Welding Schedules on Liquid Metal Embrittlement Severity,” Journal of Manufacturing Science and Engineering, vol. 141, no. 10, 2019, doi: 10.1115/1.4044099.

[17] M. Pouranvari and SPH. Marashi, “Critical review of automotive steels spot welding: process, structure and properties,” Science and Technology of welding and joining, 18(5):361–403, 2013.

[18] DR. Sigler, JG. Schroth, W. Yang, XQ. Gayden, C. Jiang, Y. Sang, and PJ. Morin, “Observations of liquid metal assisted cracking in resistance spot welds of zinc-coated advanced high strength steels,” GM Research & Development Center, Warren, page 20, 2008.

[19] P. Zhang, L. Zhu, C. Xi and J. Luo, “Study on Phase Transformation in Hot Stamping Process of USIBOR® 1500 High-Strength Steel,” Metals, 9(10), p.1119, 2019.

[20] B. H. Chang and Y. Zhou, “Numerical study on the effect of electrode force in small-scale resistance spot welding,” Journal of Materials Processing Technology, vol. 139, 1-3, 2003, doi: 10.1016/S0924-0136(03)00613-7.